Scientific Reports

https://doi.org/10.1038/s41598-026-41406-5

Article in Press

Theoretical analysis of thermomechanical response for biological skin tissues

Received: 5 January 2026

Accepted: 19 February 2026

Published online: 07 March 2026

Cite this article as: Islam N., Das B. & Lahiri A. Theoretical analysis of thermomechanical response for biological skin tissues. *Sci Rep* (2026). https://doi.org/10.1038/s41598-026-41406-5

N. Islam, B. Das & A. Lahiri

Theoretical analysis of thermomechanical response for biological skin tissues

N. Islam[1], **B. Das**[2], **and A. Lahiri**[3]

[1]Departmemt of Mathematics, Jadavpur University, Kolkata-700032, West Bengal, India
[2]Department of Mathematics, Bankura University, Bankura-722155, West Bengal, India.
[3]Departmemt of Mathematics, Jadavpur University, Kolkata-700032, West Bengal, India
[2]bappa.das1@gmail.com

ABSTRACT

This study provides an analytical investigation of the thermomechanical behavior of biological skin tissue subjected to harmonic thermal loading within the framework of four thermoelastic theories. The four employed thermoelastic theories, namely the classical dynamic coupled theory (CDC), the Lord–Shulman (LS) theory, the dual-phase-lag (DPL) theory, and the nonlocal dual-phase-lag (NLDPL) theory, are utilised to represent various heat conduction mechanisms. The governing equations are derived for skin tissues and solved using the normal mode technique in conjunction with an eigenvalue approach. Numerical simulations are conducted to analyze the distributions of temperature, displacement, and stress fields, with the results illustrated through two- and three-dimensional graphical representations. The effects of angular frequency and the nonlocal parameter on the thermomechanical response are examined in detail. A comparative evaluation of the four thermoelastic theories (CDC, LS, DPL, and NLDPL) highlights their respective capabilities under harmonic heating conditions. The findings offer valuable insights into the behavior of skin tissues under varying conditions. These results may significantly contribute to the advancement of treatments such as hyperthermia therapy and laser surgery, thereby potentially improving patient care.

Keywords:

Biological skin tissues, eigenvalue approach, harmonic heating, nonlocal bioheat equation, normal mode analysis

Introduction

The investigation of bioheat transfer in biological tissues has been an active area of research since the mid-twentieth century, primarily due to its important biomedical applications, such as hyperthermia therapy, cryosurgery, laser treatment, and thermal ablation. Accurately predicting the temperature distribution and the corresponding mechanical response is crucial for ensuring the effectiveness and safety of these medical procedures. Human skin, in particular, plays a vital role in thermal protection and regulation as it serves as the primary interface between the body and the external environment. The skin is a multilayered structure composed of the epidermis, dermis, and hypodermis, illustrated in Figure 1(b). The epidermis acts as a protective barrier, the dermis contains blood vessels, nerves, and glands that are responsible for thermoregulation, and the hypodermis provides insulation and mechanical cushioning. Due to its complex structure, strong thermo-mechanical coupling, and sensitivity to external thermal stimuli, skin tissue presents significant challenges for accurate heat transfer modeling.

The classical and most influential framework for bioheat transfer is the Pennes bioheat equation, which incorporates metabolic heat generation and blood perfusion while relying on Fourier's law of heat conduction, as proposed by Pennes [1]. Although this model has served as the foundation for numerous investigations, its assumption of infinite thermal propagation speed restricts its applicability, especially under rapid or high-frequency thermal loading conditions. To address thermo-mechanical coupling, Biot [2] introduced the coupled dynamical theory of thermoelasticity, integrating elastic deformation with heat conduction and providing enhanced congruence with experimental observations. Nonetheless, this theory still combines hyperbolic mechanical equations with parabolic heat conduction, resulting in physical inconsistencies. The Lord–Shulman (LS) theory [3], which introduces a single thermal relaxation time, circumvents the paradox of infinite heat propagation speed and enhances the realism of the analysis of transient heat transfer. Further advancements led to the dual-phase-lag (DPL) theory, independently proposed by Roy Choudhury [4] and Tzou [5], which incorporates distinct phase lags in heat flux and temperature gradient. This model effectively captures non-Fourier heat conduction phenomena and thermal wave effects, rendering it particularly applicable to microscale and biological heat transfer scenarios. Abouelregal et al. [6] proposed a new dual-phase-lag (DPL) thermoelastic model for porous materials with voids, highlighting its relevance to construction, aerospace,

and biomedical applications. The nonlocal parameter signifies an inherent material length scale linked to the microstructure of biological skin tissue, such as collagen fiber spacing and cellular dimensions. Due to the scarcity of direct experimental data for skin tissue, the parameter is assigned a magnitude comparable to the characteristic microstructural length reported in scholarly literature for soft biological tissues. It is regarded as a material-dependent constant and selected within a physically permissible range widely utilized in nonlocal thermoelastic and bioheat models. A parametric analysis is performed to investigate its impact on thermal and mechanical responses and to ensure a seamless transition from local to nonlocal behavior. Additional progress was achieved through the nonlocal dual-phase-lag (NLDPL) theory proposed by Gupta and Mukhopadhyay [7] and Eringen [8], which introduces spatial nonlocality alongside temporal phase lags. Abouelregal et al. [9] presented a generalized thermoelastic formulation incorporating Eringen's nonlocal elasticity and a fractional-order heat conduction model. This theory is particularly effective for modeling skin tissue subjected to localized or high-frequency heating, where size-dependent effects become significant.

Analytical approaches have played a crucial role in enhancing our understanding of bio-thermoelastic phenomena. Kumar et al. [10] explored temperature profiles in biological tissues exposed to external heat sources, providing valuable insights for medical applications. Hobiny and Abbas [11] utilized fractional time derivatives to investigate the thermo-mechanical interactions in living tissues subjected to sudden heating. Zenkour [12] introduced a fractional-order thermoelastic model for skin tissue under ramp-type thermal loads. Additionally, Sapa et al. [13] developed a heat conduction model based on Pennes' bioheat equation and thermodynamic principles, incorporating a single relaxation time. Bajaj et al. [14] studied the nonlinear propagation of plane waves in a gravity-affected, transversely isotropic thermoelastic half-space, offering a new perspective on this issue. Das et al. [15] analyzed the thermoelastic effects in an isotropic rectangular plate by integrating nonlocal behavior within the framework of the dual-phase-lag (DPL) heat conduction theory. Lastly, Megahid [16] examined higher-order thermal relaxation effects in skin tissue using the Moore–Gibson–Thompson (MGT) thermal model and normal mode analysis, highlighting the importance of advanced solution methods in biological heat transfer.

Numerous studies have specifically addressed the thermo-mechanical behavior of skin tissue. Hu et al. [17] investigated a finite-thickness skin layer employing a fractional dual-phase-lag bioheat model under conditions of instantaneous surface heating. Marin et al. [18] performed a numerical analysis of a nonlinear hyperbolic bioheat equation with applications to tumor treatment. Alqahtani et al. [19] introduced an analytical approach to examine thermomechanical interactions in human tissues subjected to abrupt thermal loads. Abouelregal et al. [20] proposed a fractional-order model to study heat transfer in nanomaterials by analyzing the thermoelastic vibration of one-dimensional nanostructures within the framework of nonlocal elasticity theory. Abbas et al. [21] evaluated the thermo-mechanical response of two-dimensional skin tissue under instantaneous heating, while Zhang et al. [22] applied the three-phase-lag (TPL) heat conduction model to analyze thermal wave propagation in biological tissues. Zakria et al. [23] studied a fractional-order three-phase-lag thermoelastic model to examine the effect of thermal relaxation parameters on the vibration of nonlocal thermoelastic nanobeams on Pasternak foundations. Parmar et al. [24] investigated thermal damage in skin tissue utilizing the DPL model under ramp-type heating, and Bera et al. [25] analyzed tumor tissue under electromagnetic hyperthermia, highlighting the significance of phase-lag effects. Abbas et al. [26] investigated heat transfer in living tissue during magnetic tumor hyperthermia using a nonlocal bioheat model formulated in spherical coordinates. Notwithstanding these efforts, comparative investigations that concurrently consider nonlocal effects, harmonic thermal excitation, and multiple thermoelastic theories are relatively limited.

This study examines the thermomechanical response of skin tissue, which is modeled as a one-dimensional thick plate, under harmonic heating. The investigation employs four different thermoelastic theories. The governing partial differential equations are solved using normal mode analysis and the eigenvalue approach. We present both analytical and numerical results through two- and three-dimensional graphical illustrations that depict the distribution of physical field variables in biological skin tissue. The computations are carried out using MATLAB 2021a. To validate the proposed model, we compare its results with published findings, showing strong agreement and confirming accuracy. Additionally, a comparative analysis of four thermoelastic models (CDC, LS, DPL, and NLDPL) is conducted to explore their effects on the overall thermomechanical behavior of the skin tissue. The findings reveal that angular frequency and nonlocal parameters significantly influence the thermal and mechanical responses of the skin tissue.

Basic equations for the theoretical model

Biothermoelasticity provides a comprehensive framework that combines thermoelasticity principles with bioheat conduction, offering insights into the thermomechanical behaviour of biological tissues. The governing equations for skin tissue, which include two-phase lag effects and a non-local parameter, have been thoroughly developed and examined in studies by Abbas et al. [21] and Islam et al. [27].

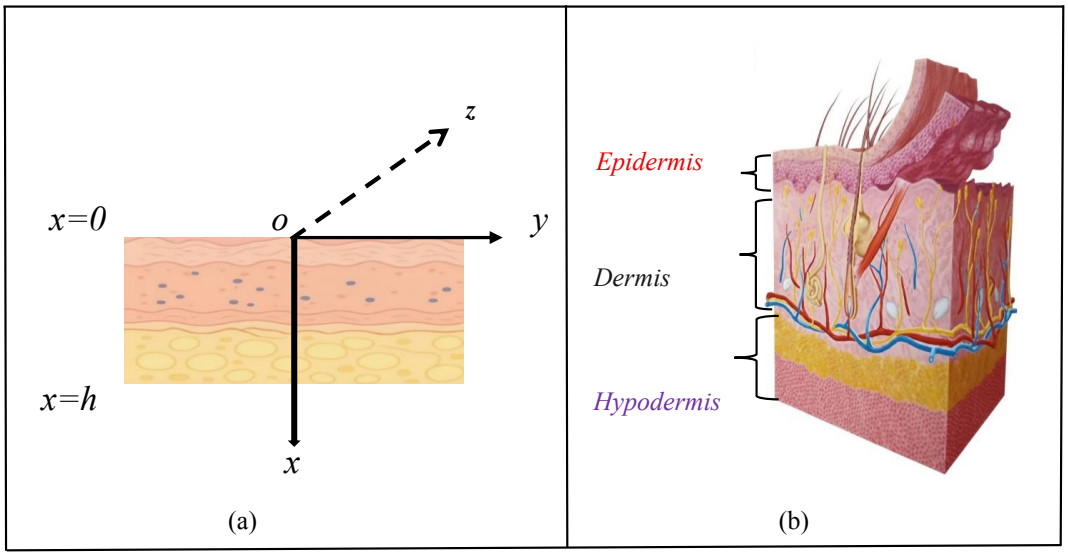

Figure 1. (a) A schematic depiction of biological skin tissue illustrates a harmonic heat source applied at the boundary surface $x = 0$, while the boundary at $x = h$ remains free of stress and temperature for any duration. (b) The skin comprises three primary layers: the epidermis, dermis, and hypodermis. Collectively, these layers serve to protect the body, assist in temperature regulation, facilitate sensory perception, and store various substances and energy.

The equation of motion is given by

$$\rho \ddot{u}_i = \mu u_{i,jj} + (\lambda + \mu) u_{j,ij} - \alpha \theta_{,i}, \tag{1}$$

where u_i is the displacement components along the coordinate axis, θ is the temperature of the tissues, ρ is the density of the tissue mass, λ and μ are Lamé's constant, $\alpha = (3\lambda + 2\mu)\alpha_\theta$ is the thermoelastic constant. Here, α_θ denotes the coefficient of thermal expansion.

The non-local bio-heat conduction in the presence of metabolic heat generation is given by

$$\kappa \left(1 + \tau_\theta \frac{\partial}{\partial t}\right) \theta_{,ii} = \left(1 + \lambda_q \frac{\partial}{\partial x} + \tau_q \frac{\partial}{\partial t}\right) \left(\rho c_e \frac{\partial \theta}{\partial t} + \alpha \theta_0 \frac{\partial}{\partial t}(u_{k,k}) - \omega_b \rho_b c_b (\theta_b - \theta) - Q_m\right), \tag{2}$$

where κ is the thermal conductivity, τ_θ and τ_q are the phase lagging parameters of the temperature gradient and the heat flux, λ_q is the nonlocal parameter, θ_0 is the reference temperature, ω_b is the blood perfusion rate, ρ_b and c_b are the density of the blood mass and specific heat, θ_b represents the blood temperature, Q_m denotes the generation of metabolic heat in the tissue cell.

The relation between stress, displacement, and temperature is given by

$$\sigma_{ij} = \mu(u_{i,j} + u_{j,i}) + (\lambda u_{k,k} - \alpha\theta)\delta_{ij}, \tag{3}$$

where σ_{ij} represent the stress components, and δ_{ij} denote the Kronecker symbol.

The strain-displacement field can be displayed as

$$e_{ij} = \frac{1}{2}(u_{i,j} + u_{j,i}). \tag{4}$$

This work introduces four different theories through the nonlocal bio-heat transportation equation (2) as follows:

(i) Classical dynamical coupled theory (CDC): $\tau_\theta = \tau_q = 0$, and $\lambda_q = 0$.
(ii) Lord and Shulman (LS) theory: $\tau_\theta = 0$, $\tau_q > 0$, and $\lambda_q = 0$.

(iii) Dual phase lag (DPL) theory: $\tau_q \geq \tau_\theta > 0$, and $\lambda_q = 0$.
(iv) Non-local dual phase lag (NLDPL) theory: $\tau_q \geq \tau_\theta > 0$, and $\lambda_q > 0$.

Validation of the Proposed Model

The accuracy and reliability of the current mathematical formulation are confirmed by checking its consistency with earlier published results in appropriate limiting scenarios. Simplifying the governing equations enables direct comparison with well-known models in the literature.

(a) **Neglecting the nonlocal parameter ($\lambda_q = 0$):**
When the non-local parameter λ_q is zero, the current model simplifies to the local thermoelastic model. In this case, Eqs. (1)–(3) match those in Alqahtani et al. [19], confirming the mathematical consistency of the nonlocal extension and showing that the model correctly reduces to classical results as a special case.

(b) **Neglecting the phase-lag parameter of the temperature gradient ($\tau_\theta = 0$) and the nonlocal parameter ($\lambda_q = 0$):**
By further setting $\tau_\theta = 0$ and $\lambda_q = 0$, the governing equations reduce to a simplified thermoelastic framework consistent with the model presented by Abbas et al. [21]. The agreement between the present results and previously published results verifies the validity, reliability, and correctness of the proposed formulation and the adopted solution methodology.

Formulation of the problem

The outer layer of the skin tissue is modeled as a one-dimensional thick plate with linear, homogeneous, and isotropic thermal properties. We have defined the coordinate system such that the x-axis stands perpendicular to the skin's surface. For our purposes, we imagine that the skin extends infinitely along both the y and z directions, as shown in Figure 1(a).

The equations (1) to (4) can be written in the following form:

$$\rho \frac{\partial^2 u}{\partial t^2} = (\lambda + 2\mu)\frac{\partial^2 u}{\partial x^2} - \alpha \frac{\partial \theta}{\partial x}, \tag{5}$$

$$\kappa \left(1 + \tau_\theta \frac{\partial}{\partial t}\right) \frac{\partial^2 \theta}{\partial x^2} = \left(1 + \lambda_q \frac{\partial}{\partial x} + \tau_q \frac{\partial}{\partial t}\right) \left(\rho c_e \frac{\partial \theta}{\partial t} + \alpha \theta_0 \frac{\partial^2 u}{\partial t \partial x} - \omega_b \rho_b c_b (\theta_b - \theta) - Q_m\right), \tag{6}$$

$$\sigma_{xx} = (\lambda + 2\mu)\frac{\partial u}{\partial x} - \alpha\theta. \tag{7}$$

The non-dimensional variables are given by

$$(x^*, u^*) = c_0 \eta_0 (x, u), (t^*, \tau_\theta^*, \tau_q^*) = c_0^2 \eta_0 (t, \tau_\theta, \tau_q), \lambda_{q_i}^* = c_0 \eta_0 \lambda_{q_i}, \sigma_{ij}^* = \frac{\sigma_{ij}}{\lambda + 2\mu}, \theta^* = \frac{\theta - \theta_b}{\theta_b}, Q_m^* = \frac{\alpha Q_m}{\rho^2 c_e {c_0}^4 {\eta_0}^2}. \tag{8}$$

where, $c_0 = \sqrt{\frac{(\lambda+2\mu)}{\rho}}$, and $\eta_0 = \frac{\rho c_e}{\kappa}$ represent the longitudinal wave speed parameter, and the thermal viscosity parameter.

Utilizing the non-dimensional equation (8), the non-dimensional forms of equations (5) - (7) are delineated as follows:

$$\frac{\partial^2 u}{\partial t^2} = \frac{\partial^2 u}{\partial x^2} - a_2 \frac{\partial \theta}{\partial x}. \tag{9}$$

$$\left(1 + \tau_\theta \frac{\partial}{\partial t}\right) \frac{\partial^2 \theta}{\partial x^2} = \left(1 + \lambda_q \frac{\partial}{\partial x} + \tau_q \frac{\partial}{\partial t}\right) \left(\frac{\partial \theta}{\partial t} + a_1 \frac{\partial^2 u}{\partial t \partial x} + a_4 \theta - Q_m\right). \tag{10}$$

$$\sigma_{xx} = \frac{\partial u}{\partial x} - a_2 \theta. \tag{11}$$

where, $a_1 = \frac{\alpha}{\rho c_E}, a_2 = \frac{\alpha\theta_0}{(\lambda+2\mu)}, a_4 = \frac{\omega_b \rho_b c_b \theta_b}{\rho c_E \eta c^2 \theta_0}$, and $e = \frac{\partial u}{\partial x}$.

Solution procedure: Normal mode analysis

To solve this problem, we use the normal mode analysis technique. This method assumes that all physical field variables change harmonically over time and can be written as products of functions that depend on space and time separately. So, the solution is expressed in this form, as explained by Das et al. [28]

$$\eta(x,t) = \eta^*(x)e^{i\omega t} \tag{12}$$

where $\eta(x,t) = [u, \theta, \sigma_{ij}]$, $\eta^*(x) = [u^*, \theta^*, \sigma^*_{ij}]$, ω is the angular frequency, $i = \sqrt{-1}$.

Using equation (12), the partial differential equations (9) and (10) convert into ordinary differential equations, which can be written as follows:

$$\frac{d^2u}{dx^2} = -\omega^2 u + a_2 \frac{d\theta}{dx}, \tag{13}$$

$$\frac{d^2\theta}{dx^2} = -\frac{ia_1\lambda_q\omega^3}{(1+i\tau_\theta\omega)}u + \frac{a_4+i\omega-\tau_q\omega^2+i\tau_q\omega a_4}{(1+i\tau_\theta\omega)}\theta + \frac{a_1\omega(i-\tau_q\omega)}{(1+i\tau_\theta\omega)}\frac{du}{dx} + \frac{\lambda_q(a_4+i\omega+a_1a_2i\omega)}{(1+i\tau_\theta\omega)}\frac{d\theta}{dx} - \frac{(1+i\omega\tau_q)}{(1+i\tau_\theta\omega)}Q_m. \tag{14}$$

The ordinary differential equations (13) and (14) can be reformulated into a vector matrix differential equation, expressed as follows:

$$\frac{dW}{dx} = AW + f \tag{15}$$

where, $W=[u \quad \theta \quad \frac{du}{dx} \quad \frac{d\theta}{dx}]^T$, $A = \begin{bmatrix} 0 & 0 & 1 & 0 \\ 0 & 0 & 0 & 1 \\ c_{31} & 0 & 0 & c_{34} \\ c_{41} & c_{42} & c_{43} & c_{44} \end{bmatrix}$, $f = [0 \quad 0 \quad 0 \quad C_{45}]^T$. where $c_{31} = -\omega^2, c_{34} = a_2$, $c_{41} = -\frac{ia_1\lambda_q\omega^3}{(1+i\tau_\theta\omega)}, c_{42} = \frac{a_4+i\omega-\tau_q\omega^2+i\tau_q\omega a_4}{(1+i\tau_\theta\omega)}, c_{43} = \frac{a_1\omega(i-\tau_q\omega)}{(1+i\tau_\theta\omega)}, c_{44} = \frac{\lambda_q(a_4+i\omega+a_1a_2i\omega)}{(1+i\tau_\theta\omega)}, c_{45} = \frac{-(1+i\omega\tau_q)}{(1+i\tau_\theta\omega)}$.

The eigenvalue approach is now employed to solve the vector-matrix differential equation (13). The characteristic equation corresponding to the coefficient matrix A is given by:

$$AX = \lambda X \tag{16}$$

Here, $X = [X_j]_{j=1,2,3,4}$ represents the set of eigenvectors corresponding to the eigenvalues $\lambda = \lambda_j$ for $j = 1, ..., 4$. The numerical computations are carried out using a programming language (MATLAB R2021a) built-in functions, which facilitate the efficient determination of both eigenvalues and their corresponding eigenvectors.

According to the regularity condition as $x \to \infty$, as discussed by Das and Lahiri [29] and Das et al. [30], the general solution of the differential equation (13) can be expressed as follows:

$$W = \sum_{j=1}^{4} X_j y_j. \tag{17}$$

where,

$$y_j = A_j e^{\lambda_j x} + e^{\lambda_j x} \int H_j e^{-\lambda_j x} dx. \tag{18}$$

$$and \;\; H_j = (B^{-1}f) \quad where \;\; B = (X_j), \; j = 1, ..., 4. \tag{19}$$

where A_j are arbitrary constants.

Hence, the corresponding expressions for the physical field variables can be written as follows:

$$(u,\ \theta\ ) = \sum_{j=1}^{4} (x_{j1}, x_{j2})(A_j e^{\lambda_j x} - \frac{H_j}{\lambda_j}). \tag{20}$$

Using this solution, equation (11) provides the expressions for the stress components, which are given as follows:

$$\sigma_{xx} = \sum_{j=1}^{4} (A_j R_{1j} - N_{1j}), \tag{21}$$

where $R_{1j} = (\lambda_j x_{j1} - a_2 x_{j2}) e^{\lambda_j x}$ and $N_{1j} = (x_{j2} a_2 H_j / \lambda_j)$.

The boundary conditions are applied to determine the values of the arbitrary constants A_j's (j=1,2,..,4).

Initial and Boundary Conditions

To evaluate the unknown constants in the analytical solution, the initial and boundary conditions corresponding to the physical model depicted in Figure 1(a) are now specified. The biological skin tissue is modeled as a finite-thickness thermoelastic layer h subjected to harmonic thermal excitation at the surface.

Initial Condition:

$$u(x,0) = \frac{\partial u(x,0)}{\partial t} = 0, \theta(x,0) = \frac{\partial \theta(x,0)}{\partial t} = 0. \tag{22}$$

Boundary Condition: The boundary conditions associated with the present problem in biological skin tissues are defined as follows-

At $x = 0$

$$\sigma_{xx}(0,t) = 0, \theta(0,t) = \theta_b sin(\omega t), t > 0, \tag{23}$$

At $x = h$

$$\sigma_{xx}(h,t) = 0, \theta(h,t) = 0. \tag{24}$$

The skin tissue is subjected to harmonic heating at the beginning of the tissue, while the surface temperature is assumed to vanish at the plane $x = h$. By using these boundary conditions, the arbitrary constants A_j's (j=1,2,..,4) are to be determined. Therefore, an analytical closed-form solution is obtained according to the consistent parametric value of the arbitrary constants, which are used in the numerical computations.

Numerical results and discussions

We now investigate the nonlocal bio-heat thermoelastic problem numerically within the framework of the four theories, such as the classical dynamic coupling (CDC) theory, Lord–Shulman (LS) theory, Dual-phase-lag (DPL) theory, and Nonlocal dual-phase-lag (NLDPL) theory. The numerical results have been illustrated through a series of two- and three-dimensional graphical representations to provide a comprehensive understanding of the thermal and mechanical responses for skin tissues and blood cells. The programming language (MATLAB R2021a) has been used as an effective computational tool to perform numerical simulations and generate the corresponding graphical output. For numerical computations, the values of the specific physical parameters used for skin tissues and blood cells are as in Abbas et al. [21], and Zenkour et al. [12, 31], which are given in tabular form in Table 1.

Significant effect under the four theories:

Figures 2 - 4 show the variation of the stress component (σ_{xx}), the temperature distribution (θ), and the dilatation (e) with the space variable (x) under four theories: CDC, LS, DPL, and NLDPL. The effects of the classical dynamical coupled theory (CDC) ($\tau_\theta = 0.0, \tau_q = 0.0, \lambda_q = 0.0$), Lord and Shulman (L-S) theory ($\tau_\theta = 0.0, \tau_q = 0.25, \lambda_q = 0.0$), the dual phase lag (DPL) theory ($\tau_\theta = 0.2, \tau_q = 0.25, \lambda_q = 0.0$), and the nonlocal dual phase lag (NLDPL) theory ($\tau_\theta = 0.2, \tau_q = 0.25, \lambda_q = 0.15$) are described in skin tissue. This section provides a comparative analysis of the significant impact of four thermoelastic theories on the behaviour of the biological skin tissue.

Table 1. Constants for materials required in numerical simulations at the reference temperature θ_0=310 K.

Property	Symbol	Value	Units
First Lamé parameter	λ	8.27×10^8	N m^{-2}
Shear modulus	μ	3.446×10^7	N m^{-2}
Density	ρ	1190	kg m^{-3}
Blood density	ρ_b	1060	kg m^{-3}
Specific heat of blood	C_b	3770	J kg^{-1} K^{-1}
Specific heat capacity	C_e	3600	J kg^{-1} K^{-1}
Thermal expansion coefficient	α_t	1×10^{-4}	K^{-1}
Thickness parameter	h	1.0	mm
Metabolic heat generation	Q_m	368.1	W m^{-3}
Blood perfusion rate	ω_b	4.0	s^{-1}
Thermal conductivity	K	0.235	W m^{-1} K^{-1}
Blood temperature	θ_b	310	K

Figure 2 illustrates the variation of normal stress (σ_{xx}) along the distance (x) in skin tissue, as analysed using four thermoelastic theories: CDC, LS, DPL, and NLDPL. The stress profiles exhibit a symmetric trend: decreasing in the range $0 \leq x \leq 0.5$ and increasing in the range $0.5 \leq x \leq 1.0$. The LS and DPL theories yield closely aligned results, indicating similar stress predictions. The CDC model shows comparatively higher stress magnitudes. The NLDPL theory demonstrates a smoother and more moderate stress distribution, attributed to its incorporation of nonlocal and microstructural effects. This highlights the NLDPL model's enhanced capability to accurately capture the mechanical behaviour of biological tissues under thermal loading conditions.

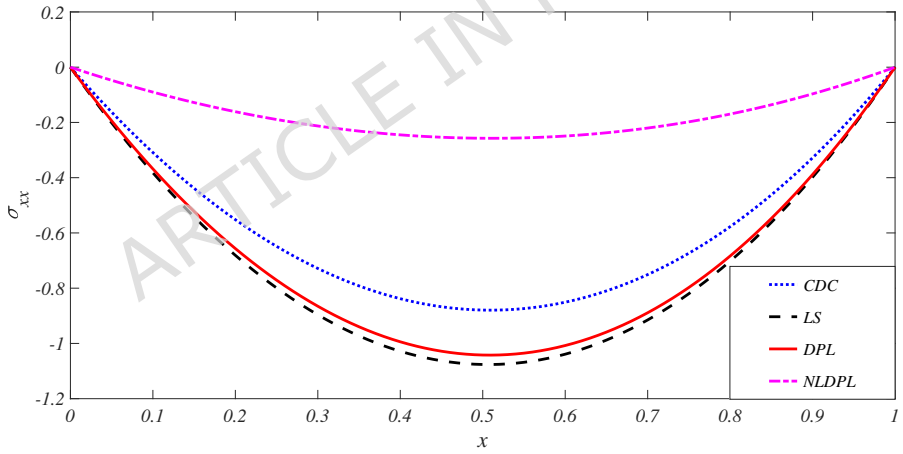

Figure 2. The variation of the normal stress component (σ_{xx}) along the distance (x) for four theories.

Figure 3 illustrates the variation of the temperature distribution (θ) with dimensionless distance (x) within skin tissue, as analysed through various thermoelastic theories: Classical Dynamical Coupled (CDC), Lord–Shulman (LS), Dual Phase Lag (DPL), and Non-Local Dual Phase Lag (NLDPL). The findings suggest that the CDC theory tends to overestimate temperature during transient states, making it less suitable for sophisticated biomedical applications, such as laser surgery or hyperthermia therapy. The NLDPL theory exhibits more effective heat dissemination owing to its consideration of microstructural interactions, thereby underscoring its potential for enhanced accuracy in biomedical applications. The LS theory demonstrates improved performance under short-pulse heating conditions but still faces limitations in accurately capturing the thermal behaviour of heterogeneous biological tissues.

Figure 4 illustrates the variation in cubical dilatation (e) across a dimensionless distance (x) within skin tissue, as forecasted by four distinct thermoelastic theories: Classical Dynamical Coupled (CDC), Lord-Shulman (LS), Dual Phase Lag (DPL), and Non-Local Dual Phase Lag (NLDPL). The influence of the cubical dilatation (e) in the contexts of DPL and NLDPL is

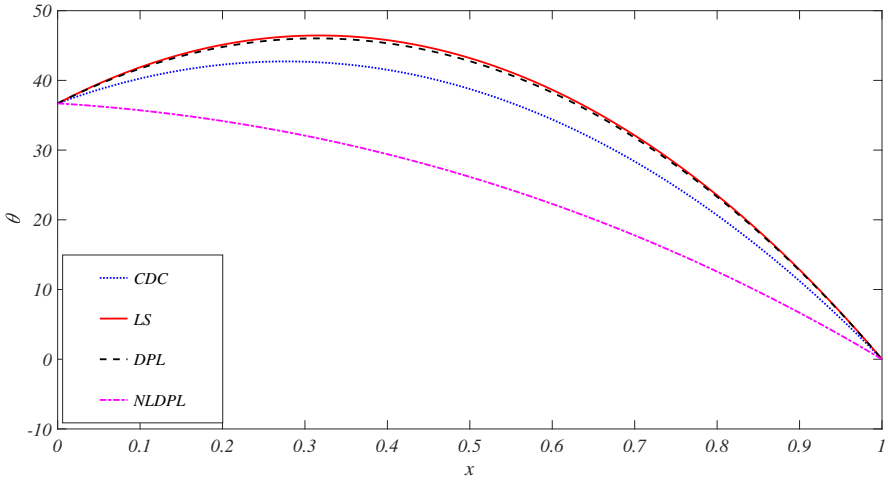

Figure 3. The temperature distribution (θ) along the distance (x) for four theories.

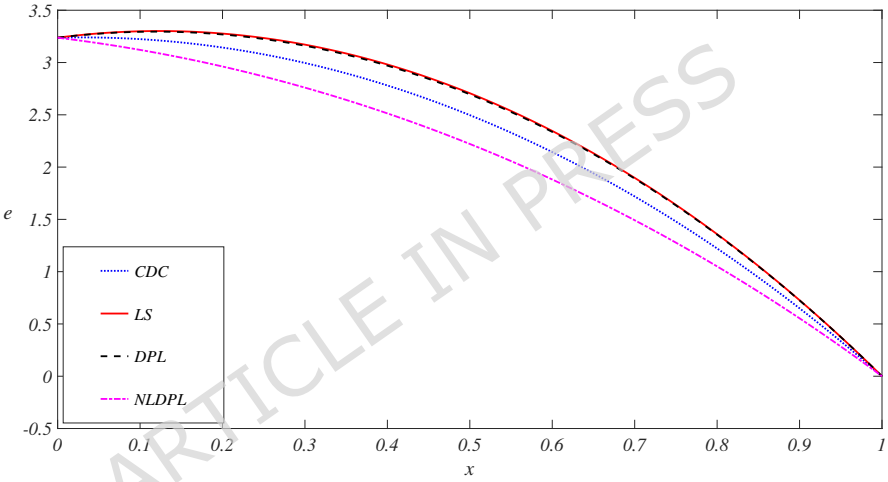

Figure 4. Variation of the cubical dilatation (e) along the distance (x) under the four thermoelastic theories.

notably advanced, effectively capturing wave-like heat transfer phenomena and nonlocal strain effects, which are pivotal for applications such as laser surgery, hyperthermia therapy, and ultrasound procedures. This figure demonstrates that the more sophisticated models (DPL, NLDPL) provide enhanced accuracy when modelling the thermal and mechanical responses of skin tissue under stress. Notably, NLDPL yields the most realistic predictions by integrating phase lags and non-local interactions, making it especially advantageous for biomedical applications.

The analysis of Figures 2 to 4 emphasises that the NLDPL theory offers the most precise and realistic predictions of thermoelastic responses in skin tissue by integrating both phase-lag effects and non-local interactions. In comparison with the CDC, LS, and DPL models, the NLDPL model more effectively characterises stress, temperature variations, and cubic dilatation behaviour under thermal loading conditions. Consequently, this model is particularly suitable for advanced biomedical applications, including laser treatment, hyperthermia, and tissue engineering.

To facilitate quantitative benchmarking and enable direct comparison among different thermoelasticity models, the numerical values of the normal stress (σ_{xx}), temperature distribution (θ), and cubical dilatation (e) at selected spatial locations are presented in Table 2.

The numerical results presented in Table 2 pertain to the same material properties, boundary conditions, and spatial coordinates as those utilized in the graphical representations. The table emphasizes the quantitative distinctions among the

Table 2. Benchmark numerical values of the normal stress (σ_{xx}), temperature distribution (θ), and cubical dilatation (e) at selected spatial locations for different thermoelasticity models (CDC, LS, DPL, and NLDPL).

	x (mm)	CDC	LS	DPL	NLDPL
σ_{xx}	0.1	-0.327676	-0.394877	-0.383572	-0.028689
	0.5	-0.922320	-1.104010	-1.075510	-0.085644
	0.9	-0.340152	-0.405454	-0.396898	-0.033469
θ	0.1	40.26430	41.87880	41.69320	35.70800
	0.5	38.76340	43.19910	42.75610	26.15520
	0.9	11.21970	12.83830	12.72100	6.65990
e	0.1	3.224860	3.300110	3.295040	3.121840
	0.5	2.497720	2.707470	2.696880	2.222020
	0.9	0.649772	0.727279	0.725486	0.554129

examined thermoelasticity models and supplies dependable benchmark data for subsequent analytical and numerical evaluations.

Significant effect of the angular frequency (ω):

Figures 5 - 7 represent the variations of the normal stress component (σ_{xx}), temperature distribution (θ), and the cubical dilatation (e) along the distance x according to fixed values of the angular frequency ($\omega = 0.80, 0.85, 0.90, 0.95$). The fixed values of other parameters are $\tau_\theta = 0.2$, $\tau_q = 0.25$, and $\lambda_q = 0.15$. In this section, we discussed the significant influence of the angular frequency on the behavior of the biological skin tissue.

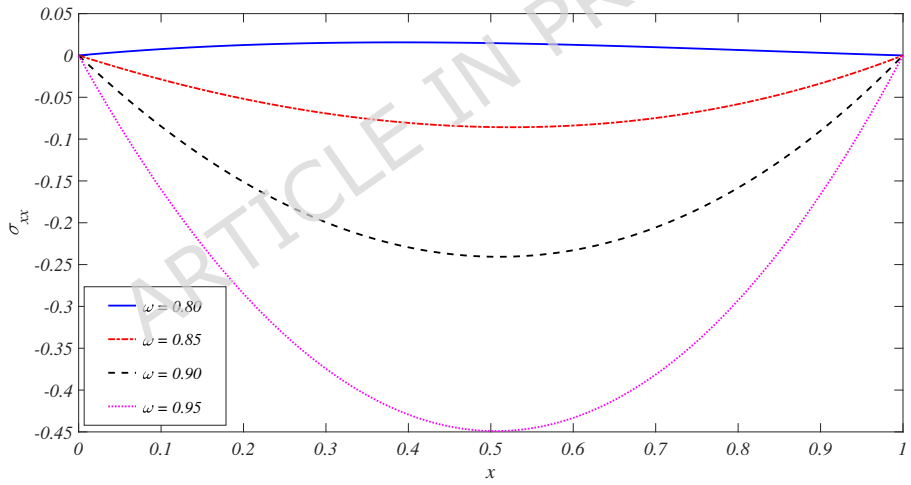

Figure 5. The variation of the normal stress component (σ_{xx}) along the distance (x) for fixed four values of the angular frequency(ω).

Figure 5 depict the normal stress component (σ_{xx}) varies along the spatial coordinate x for different angular frequencies ($\omega = 0.80, 0.85, 0.90, 0.95$). When $\omega = 0.90$ and $\omega = 0.95$, the normal stress (σ_{xx}) decreases from $x = 0$ to 0.5, then increases from 0.5 to 1.0. In both cases, the stress stays negative throughout, indicating a compressive response. At $\omega = 0.80$, σ_{xx} remains positive everywhere, reflecting a tensile behavior. This suggests that at lower frequencies, thermal expansion dominates, preventing the formation of compressive stress regions. For $\omega = 0.85$, the stress distribution shows intermediate behavior between the tensile response at 0.80 and the compressive response at higher frequencies. Overall, these results underscore the significant impact of angular frequency on the stress distribution and the thermoelastic response of the medium.

Figure 6 shows the temperature distribution (θ) with the space variable (x), representing the depth of the skin tissue. The temperature decreases gradually from the tissue surface ($x = 0$) to the deeper boundary ($x = 1$) for all values of the angular frequency ($\omega = 0.80, 0.85, 0.90, 0.95$). Higher values of ω are also observed to lead to a noticeable increase in surface

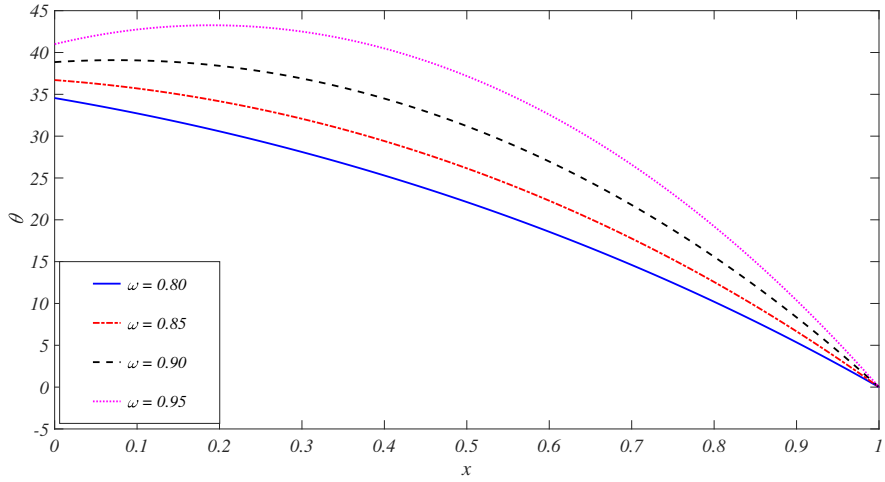

Figure 6. The temperature distribution (θ) along the distance (x) for fixed four values of the angular frequency(ω).

temperature. In particular, the maximum temperature at $x = 0$ rises from approximately $\theta = 34$ for $\omega = 0.80$ to about $\theta = 41$ for $\omega = 0.95$. These results highlight the strong influence of the frequency parameter on the thermal response, which is important to regulate the thermal dosage in treatments.

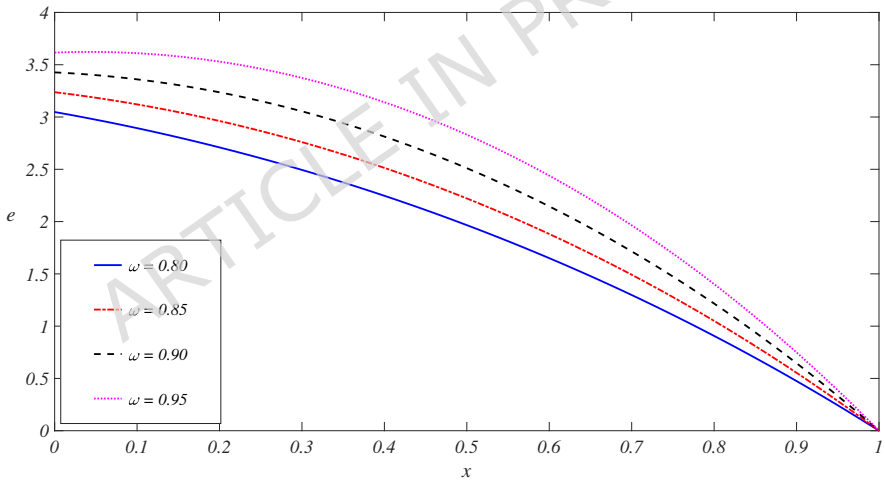

Figure 7. Variation of the cubical dilatation (e) along the distance (x) for fixed four values of the angular frequency(ω).

Figure 7 illustrates the variation of the cubical dilatation (e) with respect to the space variable (x) for different angular frequencies $(\omega = 0.80, 0.85, 0.90, 0.95)$ under a harmonic heating boundary condition applied to the skin tissue. The results show that the cubical dilatation (e) gradually decreases across the space domain for all the frequencies considered. As the angular frequency increases from $\omega = 0.80$ to $\omega = 0.95$, the magnitude of volumetric stress consistently rises throughout the tissue. This shows a clear relationship between the frequency of excitation and the amplitude of tissue deformation. Such behavior is commonly encountered in studies involving wave propagation, acoustic fields, and mechanical vibrations in soft biological tissues.

The results presented in Figures 5 - 7 demonstrate that angular frequency (ω) has a significant impact on the thermoelastic behavior of skin tissue under harmonic thermal loading. These findings indicate that higher excitation frequencies intensify both thermal and mechanical effects in biological tissues, which is essential for understanding dynamic thermal therapies and designing biomedical applications involving periodic heating.

Significant effect of the Non-local parameter (λ_q) :

Figures 8 - 10 describe the normal stress component(σ_{xx}), temperature distribution (θ) and the cubical dilatation (e) with the space variable(x) for fixed values of the non-local parameter ($\lambda_q = 0.015, 0.025, 0.035, 0.045$). The fixed values of other parameters are $\tau_\theta = 0.2$ and $\tau_q = 0.25$. In this section, we discussed the significant impact of the non-local parameter on the skin tissue.

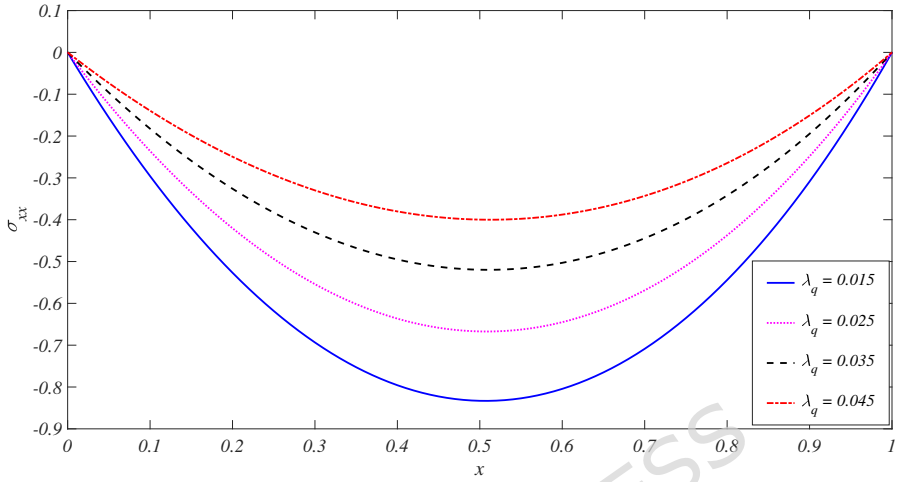

Figure 8. The variation of the normal stress component (σ_{xx}) along the distance (x) for fixed values of the non-local parameter(λ_q).

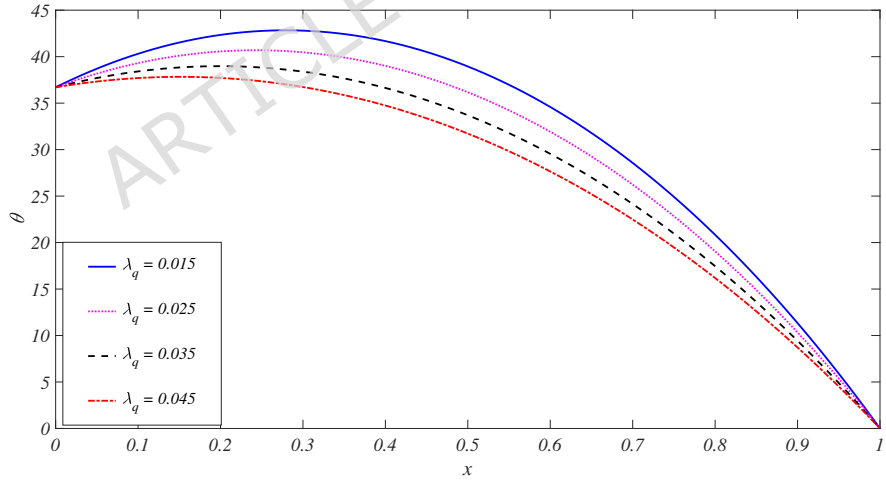

Figure 9. The temperature distribution (θ) along the distance (x) for fixed values of the non-local parameter(λ_q).

Figure 8 illustrates the variation of the normal stress component (σ_{xx}) with respect to the space variable (x) for fixed values of the non-local parameter (λ_q=0.015, 0.025, 0.035, and 0.045) in biological skin tissue. The analysis is conducted under harmonic thermal excitation, assuming zero-stress boundary conditions at both ends of the tissue. The results show that the normal stress is symmetric and reaches its peak at the minimum value at the point $x = 0.5$, reducing to zero at the boundaries. As λ_q increases, the magnitude of the stress diminishes, indicating that stronger non-local interactions lead to a smoothing effect in the stress distribution. This behavior highlights the influence of the non-local parameter in modulating internal stress responses in thermally loaded biological materials.

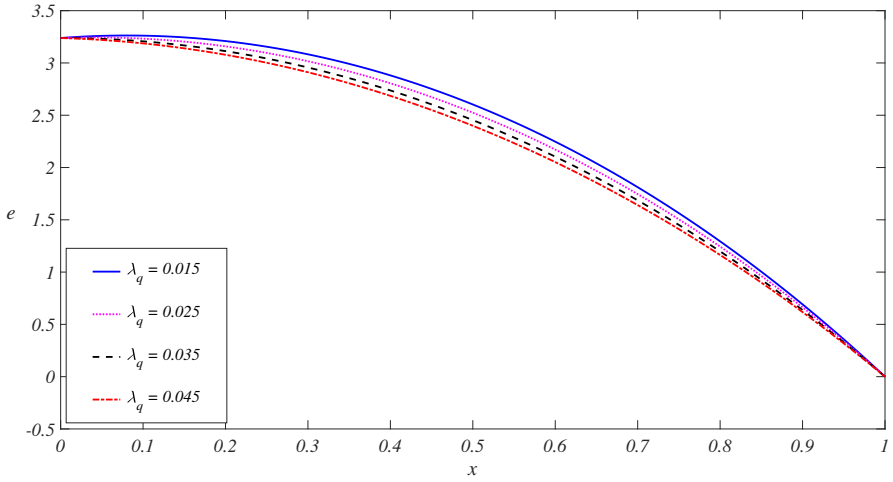

Figure 10. Variation of the cubical dilatation (e) along the distance (x) for fixed values of the non-local parameter(λ_q).

Figure 9 illustrates the temperature distribution (θ) along the space variable (x) within a biological skin tissue subjected to harmonic heating, for selected values of the non-local parameter (λ_q= 0.015, 0.025, 0.035, and 0.045). The thermal boundary conditions are applied such that the temperature is prescribed at both ends of the tissue. The results indicate that the temperature initially increases slightly, reaches a peak, and then gradually decreases toward the boundary. As the non-local parameter λ_q increases, the overall temperature within the skin tissue decreases. This implies that the presence of stronger non-local effects reduces the thermal response, acting to dissipate the heat more efficiently across the domain. The comparison among different values of λ_q demonstrates the influence of non-local thermal conductivity on the internal temperature profile of the skin tissue under transient heating.

Figure 10 illustrates the variation of the cubical dilatation (e) with respect to the space variable (x) within the skin tissue, for fixed values of the non-local parameter (λ_q = 0.015, 0.025, 0.035, and 0.045). It is observed that the cubical dilatation gradually diminishes along the spatial domain. As the value of λ_q increases, the cubical dilatation values exhibit a slight decrease, suggesting that non-local effects mitigate the volumetric expansion of the tissue. The inset offers a magnified view of the region surrounding x = 0.45 to 0.50, where the differences between the curves are more discernible. This behavior indicates that higher non-local parameter values tend to suppress the mechanical deformation caused by thermal loading. The results underscore the significance of considering non-local interactions in the analysis of the thermoelastic behavior of skin tissue.

The analysis of Figures 8 - 10 reveals that the non-local parameter (λ_q) significantly influences the thermoelastic response of skin tissue under harmonic thermal excitation. As λ_q increases, both the normal stress and the cubical dilatation decrease in magnitude, while the temperature distribution becomes smoother and lower in intensity. These findings emphasize the role of non-local effects in moderating thermal and mechanical behavior, which is crucial for accurate modeling of biological tissues in biomedical applications.

Significant effect of three-dimensional distributions for the normal stress, temperature, displacement, and the cubical dilatation:

Figures 11 - 14 illustrate the variation of the normal stress component (σ_{xx}), the temperature distribution (θ), displacement component (u), and the cubical dilatation (e) along the distance (x) and time variable (t). The fixed values of other parameters are $\tau_\theta = 0.2$, $\tau_q = 0.25$, and $\lambda_q = 0.15$. In this section, the three-dimensional effects on biological skin tissue are examined in detail.

Figure 11 illustrates the variation of the normal stress component (σ_{xx}) with the space variable (x) and the time variable (t) within skin tissue. The stress distribution displays a smooth, concave profile, wherein σ_{xx} attains its maximum compressive value near the midpoint of both spatial and temporal domains. The surface plot demonstrates that the normal stress increases gradually from the central region toward the boundaries along both spatial and temporal dimensions. The colour gradient enhances the visualization of stress intensity within the domain, indicating that thermal and mechanical interactions within the tissue evolve symmetrically with respect to both space and time. This behaviour underscores the coupled thermoelastic

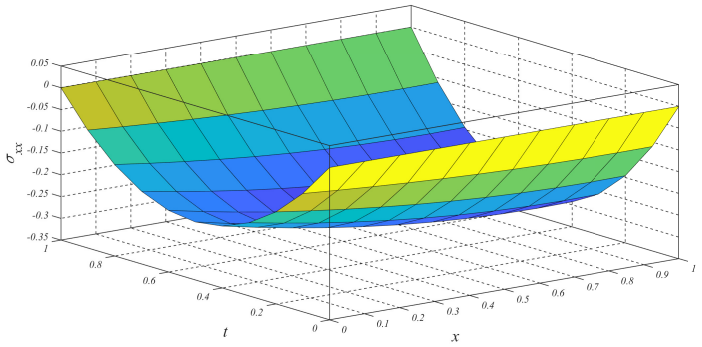

Figure 11. The variation of the normal stress component (σ_{xx}) along the distance (x) and time variable (t).

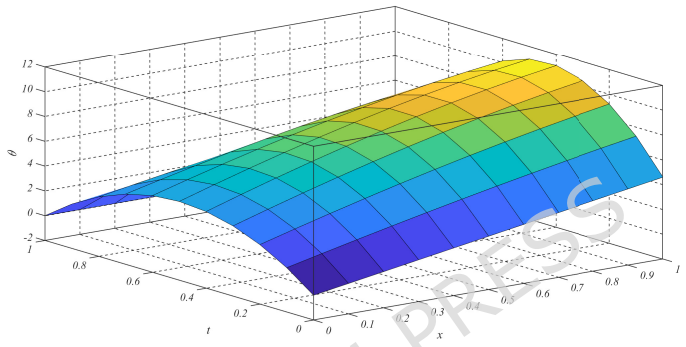

Figure 12. The temperature distribution (θ) along the distance (x) and time variable (t).

response of the skin under transient loading conditions, emphasizing the significance of temporal and spatial effects on stress distribution in biological tissues.

Figure 12 depicts the temperature distribution (θ) as a function of the space coordinate (x) and time coordinate (t) within skin tissue. The temperature exhibits a gradual increase over time, demonstrating a clear propagation of heat from the boundary towards the interior of the tissue. Initially, the temperature remains low throughout the domain; however, it steadily rises as time advances, indicative of effective heat diffusion. The surface profile is smooth and continuous, emphasizing the thermal response of skin under transient heating conditions. This behavior is essential for understanding heat distribution in biological tissues and holds particular relevance for medical procedures such as thermal therapy and diagnostic applications involving heat transfer.

Figure 13 illustrates the displacement component (u) as a function of the space variable (x) and the time variable (t). The displacement consistently remains negative, indicative of a compressive effect across the tissue. As both time and spatial coordinates increase, the displacement intensifies before gradually diminishing in magnitude, suggesting a recovery process. This pattern signifies that the skin tissue exhibits a mechanical response to thermal influences. The smooth contour of the graph suggests a stable and continuous variation in displacement, emphasizing the impact of thermoelastic interactions over temporal and spatial domains. Overall, the figure offers valuable insights into the deformation behavior of skin tissue under coupled thermal and mechanical conditions.

Figure 14 illustrates the variations in cubical dilatation (e) as a function of the space variable (x) and the time variable (t) within the skin tissue. As both time and space increase, the cubical dilatation correspondingly elevates smoothly, signifying a gradual expansion of the tissue attributable to thermal effects. The surface plot illustrates how the expansion begins slowly and gradually increases over time before eventually decreasing. This pattern reflects the tissue's response to thermal load and provides valuable information on the evolution of deformation in the skin under such conditions. These findings contribute to the understanding of thermoelastic behavior in biomedical and thermal applications that involve soft tissues.

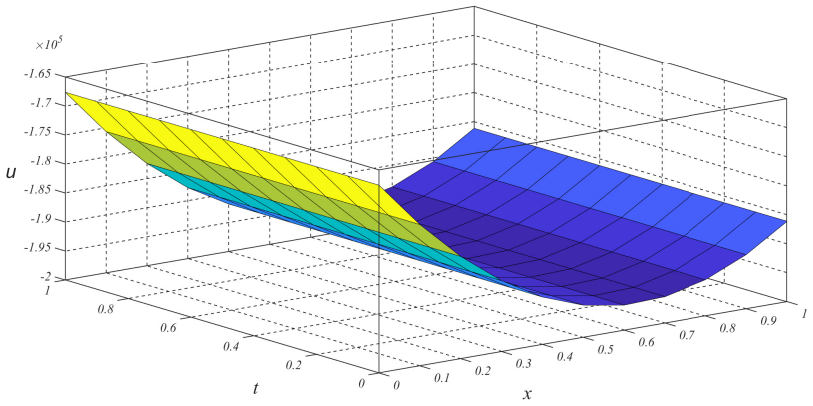

Figure 13. The displacement component (u) along the distance (x) and time variable (t).

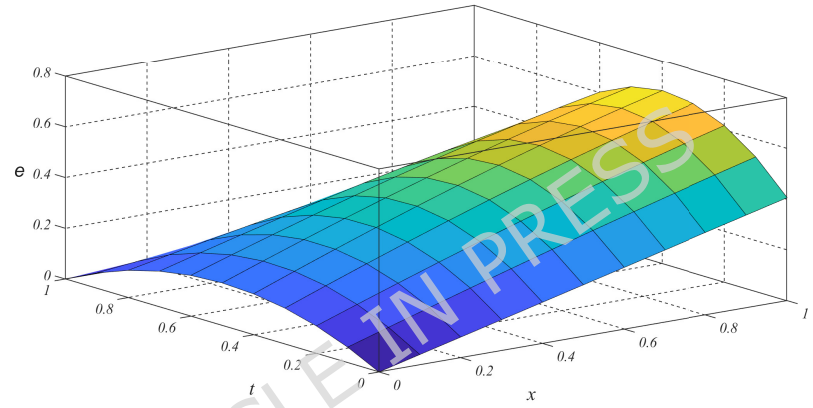

Figure 14. Variation of the cubical dilatation (e) along the distance (x) and time variable (t).

Figures 11 - 14 demonstrate the significant influence of coupled thermoelastic effects on skin tissue under transient thermal loading. The observed variations in stress, temperature, displacement, and the cubical dilatation reveal a smooth and consistent response, indicating that thermal and mechanical interactions play a critical role in tissue deformation and heat propagation. These findings are crucial for understanding biothermal behaviour in medical and biological applications.

Conclusion

This study presents a comprehensive analysis of the biothermal response of skin tissue, modeled as a one-dimensional thick plate subjected to harmonic thermal loading, within the framework of four distinct thermoelastic theories. Employing normal mode analysis combined with the eigenvalue approach, the variations in key physical field variables, including temperature, displacement, cubical dilatation, and stress, were systematically examined. The numerical results, illustrated graphically, reveal the significant effects of the angular frequency (ω) and the nonlocal parameter (λ_q) on the thermoelastic behavior of skin tissue. A comparative evaluation of four thermoelastic models (CDC, LS, DPL, and NLDPL) demonstrates the improved accuracy and effectiveness of the nonlocal dual-phase-lag (NLDPL) model in capturing coupled thermal and mechanical phenomena in biological tissues.

The key observations are summarized as follows:

i) The numerical analysis of the nonlocal bioheat transfer model yields valuable insights and highlights distinct improvements compared with the CDC, LS, DPL, and NLDPL models.

ii) The results indicate that the angular frequency (ω) has a significant influence on the thermoelastic behavior of the skin tissue.

iii) The analysis shows that the nonlocal parameter (λ_q) plays a critical role in influencing the thermoelastic response of the skin tissue under harmonic thermal excitation.

iv) Variations in normal stress, temperature, displacement, and cubical dilatation are smooth and consistent, indicating the important interplay between thermal and mechanical effects in the skin tissue deformation and heat propagation.

v) Hyperthermia offers an exciting possibility as a treatment approach. By gently warming tumor tissues to between 40 °C and 44 °C, especially above 42.5 °C, we can increase the susceptibility of cancer cells to heat-induced apoptosis. The treatment tends to be more effective at higher temperatures, making it a promising area of ongoing research.

These findings enhance the understanding of how biological skin tissue responds to thermal and mechanical loads, which is essential for medical applications such as laser therapy, thermal imaging, and hyperthermia. By analysing stress, temperature, displacement, and volumetric dilatation using advanced thermoelastic models, researchers can more precisely predict tissue behavior under various conditions. This knowledge underpins the development of safer and more effective clinical treatments, contributing to an enhanced understanding of tissue response in biomedical applications.

Acknowledgments

The authors express gratitude to the reviewers for their suggestions, which have improved the current work.

Funding

This research did not receive any kind of funding.

Data Availability

All data generated or analyzed in this study are included in the article. The computational work presented has been carried out using MATLAB (R2021a).

Disclosure statement

The authors declare that they have no known competing financial or non-financial interests that could have appeared to influence the work reported in this paper.

References

1. Pennes, H.H., 1948. Analysis of tissue and arterial blood temperatures in the resting human forearm. Journal of applied physiology, 1(2), pp.93-122. https://doi.org/10.1152/jappl.1948.1.2.93
2. Biot, M.A., 1956. Thermoelasticity and irreversible thermodynamics. Journal of Applied Physics, 27(3), pp.240-253. https://doi.org/10.1063/1.1722351
3. Lord, H.W. and Shulman, Y., 1967. A generalized dynamical theory of thermoelasticity. Journal of the Mechanics and Physics of Solids, 15(5), pp.299-309. https://doi.org/10.1016/0022-5096(67)90024-5
4. Choudhuri, S.R., 2007. On a thermoelastic three-phase-lag model. Journal of Thermal Stresses, 30(3), pp.231-238. https://doi.org/10.1080/01495730601130919
5. Tzou, D.Y., 1995. A unified field approach for heat conduction from macro-to micro-scales. Journal of Heat Transfer, 117(1), pp.8-16. https://doi.org/10.1115/1.2822329
6. Abouelregal, A.E., Civalek, Ö., Akgöz, B., Foul, A. and Askar, S.S., 2025. Analysis of thermoelastic behavior of porous cylinders with voids via a nonlocal space-time elastic approach and Caputo-tempered fractional heat conduction. Mechanics of Time-Dependent Materials, 29(2), pp.1-32. https://doi.org/10.1007/s11043-025-09770-3
7. Gupta, M. and Mukhopadhyay, S., 2019. A study on generalized thermoelasticity theory based on non-local heat conduction model with dual-phase-lag. Journal of Thermal Stresses, 42(9), pp.1123-1135. https://doi.org/10.1080/01495739.2019.1614503

8. Eringen, A.C., 1974. Theory of nonlocal thermoelasticity. International Journal of Engineering Science, 12(12), pp.1063-1077. https://doi.org/10.1016/0020-7225(74)90033-0
9. Abouelregal, A.E., Akgöz, B. and Civalek, Ö., 2022. Nonlocal thermoelastic vibration of a solid medium subjected to a pulsed heat flux via Caputo–Fabrizio fractional derivative heat conduction. Applied Physics A, 128(8), p.660. https://doi.org/10.1007/s00339-022-05786-5
10. Kumar, D., Singh, S. and Rai, K.N., 2016. Analysis of classical Fourier, SPL and DPL heat transfer model in biological tissues in the presence of metabolic and external heat source. Heat and Mass Transfer, 52(6), pp.1089-1107. https://doi.org/10.1007/s00231-015-1617-0
11. Hobiny, A. and Abbas, I., 2023. The effect of fractional derivatives on thermo-mechanical interaction in biological tissues during hyperthermia treatment using eigenvalues approach. Fractal and Fractional, 7(6), p.432. https://doi.org/10.3390/fractalfract7060432
12. Zenkour, A.M., Saeed, T. and Al-Raezah, A.A., 2023. A 1D thermoelastic response of skin tissue due to ramp-type heating via a fractional-order Lord–Shulman model. Journal of Computational Applied Mechanics, 54(3), pp.365-377. https://doi.org/10.22059/jcamech.2023.364796.871
13. El-Sapa, S., El-Bary, A.A., Albalawi, W. and Atef, H.M., 2024. Modelling Pennes' bioheat transfer equation in thermoelasticity with one relaxation time. Journal of Electromagnetic Waves and Applications, 38(1), pp.105-121. https://doi.org/10.1080/09205071.2023.2272612
14. Bajaj, S., Shrivastav, A.K., Somvanshi, A. and Saini, G.L., 2025. Effect of gravity and variable thermal conductivity in a thermoelastic half space with dual phase lag model. Scientific Reports, 15, p.44362. https://doi.org/10.1038/s41598-025-28050-1
15. Das, B., Islam, N. and Lahiri, A., 2025. Study of non-local thermoelasticity of a rectangular plate. Journal of Thermal Stresses, 48(2), pp.186-208. https://doi.org/10.1080/01495739.2025.2466099
16. Megahid, S.F., 2025. Two-dimensional biothermomechanical effects in a layer of skin tissue exposed to variable thermal loading using a fourth-order MGT model. Scientific Reports, 15(1), pp.1-21. https://doi.org/10.1038/s41598-025-01745-1
17. Hu, Y., Zhang, X.Y. and Li, X.F., 2022. Thermoelastic response of skin using time-fractional dual-phase-lag bioheat heat transfer equation. Journal of Thermal Stresses, 45(7), pp.597-615. https://doi.org/10.1080/01495739.2022.2078452
18. Marin, M., Hobiny, A. and Abbas, I., 2021. Finite element analysis of nonlinear bioheat model in skin tissue due to external thermal sources. Mathematics, 9(13), p.1459. https://doi.org/10.3390/math9131459
19. Alqahtani, Z., Abbas, I.A., El-Bary, A.A. and Almuneef, A., 2024. Analytical solutions of thermomechanical interaction in living tissues under dual phase-lag model. Indian Journal of Physics, 98(14), pp.4663-4669. https://doi.org/DOI:10.1007/s12648-024-03245-w
20. Abouelregal, A.E., Civalek, O. and Akgoz, B., 2025. A size-dependent non-fourier heat conduction model for magneto-thermoelastic vibration response of nanosystems, 11(2), pp. 344-357. https://doi.org/10.22055/jacm.2024.46746.4584
21. Abbas, I.A., El-Bary, A.A. and Mohamed, A.O., 2024. Generalized thermomechanical interaction in two-dimensional skin tissue using eigenvalues approach. Journal of Thermal Biology, 119, p.103777. https://doi.org/10.1016/j.jtherbio.2023.103777
22. Zhang, Q., Sun, Y. and Yang, J., 2020. Bio-heat response of skin tissue based on three-phase-lag model. Scientific Reports, 10(1), p.16421. https://doi.org/10.1038/s41598-020-73590-3
23. Zakria, A., Yahya, A., Saidi, A., Suhail, M., Rabih, M.N.A. and Osman, O.A.A., 2025. Response of nonlocal thermoelastic nanobeams supported by Pasternak foundations to the effect of generalized fractional theory with three-phase lags. Scientific Reports, 15(1), p.22317. https://doi.org/10.1038/s41598-025-00987-3
24. Parmar, P., Karmakar, S., Lahiri, A. and Sarkar, S.P., 2025. Study of the generalized two-dimensional bioheat problem in the context of memory-dependent derivative. Journal of Thermal Biology, 129, p.104107. https://doi.org/10.1016/j.jtherbio.2025.104107
25. Bera, A., Dutta, S., Misra, J.C. and Shit, G.C., 2021. Computational modeling of the effect of blood flow and dual phase lag on tissue temperature during tumor treatment by magnetic hyperthermia. Mathematics and Computers in Simulation, 188, pp.389-403. https://doi.org/10.1016/j.matcom.2021.04.020
26. Abbas, I., Hobiny, A. and El-Bary, A., 2024. Numerical solutions of nonlocal heat conduction technique in tumor thermal therapy. Acta Mechanica, 235(4), pp.1865-1875. https://doi.org/10.1007/s00707-023-03803-z

27. Islam, N., Das, B., Shit, G.C. and Lahiri, A., 2025. Thermoelastic and electromagnetic effects in a semiconducting medium. Acta Mech 236, pp.2171–2191. https://doi.org/10.1007/s00707-025-04267-z

28. Das, B., Islam, N. and Lahiri, A., 2024. Analytical study of micropolar thermoelastic rectangular plate under three theories. Journal of Thermal Stresses, 47(4), pp.521-536. https://doi.org/10.1080/01495739.2024.2314062

29. Das, B. and Lahiri, A., 2015. Generalized magnetothermoelasticity for isotropic media. Journal of Thermal Stresses, 38(2), pp.210-228. https://doi.org/10.1080/01495739.2014.985564

30. Das, B., Islam, N. and Lahiri, A., 2025. Comparative thermoelastic analysis of semiconductors with an external heat source under three theories. Scientific Reports, 15(1), p.40120. https://doi.org/10.1038/s41598-025-23984-y

31. Zenkour, A.M., Saeed, T. and Alnefaie, K.M., 2023. Analysis of the bio-thermoelasticity response of biological tissues subjected to harmonic heating using a refined Green–Lindsay model. Journal of Computational Applied Mechanics, 54(4), pp.588-606. https://doi.org/10.22059/jcamech.2023.366508.889